Study of Co-Injection Processes using Viscous Newtonian Fluids in a Hele-Shaw Cell

Undergraduate Honors Thesis

Presented in Partial Fulfillment of the Requirements for the Graduation with Honors Research Distinction in the College of Engineering at The Ohio State University

By

Matthew David Ellison

William G. Lowrie Department of Chemical and Biomolecular Engineering

The Ohio State University

2017

Thesis Committee:

Dr. Kurt W. Koelling, Advisor

Dr. David Tomasko

Abstract

Co-injection molding incorporates the use of two or more immiscible polymers to make a singular part. Industrially, this process is accomplished by injecting one material within another to create a skin and core combination. This allows for the creation of parts that combine desirable characteristics such as rigidity and flexibility seen in products ranging from toothbrushes to phone cases. In addition, this process is used to create plastics that combine virgin and recycled material without sacrificing durability through degradation. To better understand the influence of viscosity and surface tension in the co-injection process, a Hele-Shaw cell, consisting of two long plates separated by a narrow gap is used to represent the 2-dimensional analog to the industrial process. Prior experimentation with the Hele-Shaw cell was used to model the gas-assisted injection molding (GAIM) process where only one plastic is injected into the mold followed by an air bubble to create a hollow part. The goal of this project is to expand previous studies to include the co-injection process. Testing analyzes the viscosity ratio between the penetrating and displaced fluids. Industrially, co-injection is used to create a wide array of parts. Since these parts are costly to test individually, this research will contribute to a better understanding and prediction of the fluid interaction within the process and decrease process cost. In addition, this study is applicable to the problems faced in enhanced oil recovery where chemical injection is used.

Acknowledgments

I would like to thank my research advisors, Dr. Koelling, and Varun Venoor, for their instruction, guidance and assistance throughout the course project. Their advice was instrumental in paving the way for success during this project. I would also like to express my appreciation for the support and encouragement provided by Charlotte Tan along with my family and friends. Finally, I would like to thank the Undergraduate Research Scholarship committee for their financial support of this project.

Vita

2013……. William Mason High School

2017…… B.S. Chemical and Biomolecular Engineering, The Ohio State University

Fields of Study

Major Field: Chemical and Biomolecular Engineering

Table of Contents

List of Tables

List of Figures

Chapter 1: Introduction

The penetration of a bubble through a Newtonian fluid contained in a Hele-Shaw cell is a problem with practical applications in co-injection molding, gas-assisted injection molding and in the polymer flooding method for enhanced oil recovery. Polymer-augmented flooding water uses an aqueous polymer solution as a driving fluid to push viscous oil out of wells after the initial recovery has been completed. The potential for recovery using this method is often reduced by an interfacial 'viscous fingering' instability, which reduces sweep efficiencies and recoveries [1]. Gas-assisted injection molding is an innovative polymer processing operation, in which a mold is partially filled with a polymer melt, followed by injection of high-pressure nitrogen gas to fill out the mold. This two-step process results in hollow parts with reduced weight, higher strength-weight ratio, reduced frozen-in stresses, and higher surface finish quality. One drawback to this process, however, is the unwanted protrusion, or fingering, of the nitrogen gas bubble into thin-walled sections of the part, which can cause a subsequent decrease in part strength. Likewise, co-injection molding incorporates a two-step filling process of two different polymers. The second polymer injection is concentric with the first creating a shell and core combination between the two

polymers. Additional injections can follow to create a layering of multiple shells under this method. Using this technique parts can be manufactured with a combination of desirable characteristics between the selection of polymers used. Additionally, this technique allows for the combination of virgin and recycled polymer to be incorporated together without sacrificing the overall durability and integrity of the part.

This current work is directed at understanding some of the complex phenomena that occur at the liquid-liquid interface, which causes this fingering. The two-step process is studied by using two viscous Newtonian fluids contained in a Hele-Shaw flow cell.

Extensive research has gone into the interactions between a gas-liquid interface in a Hele-Shaw cell. Some of the first studies of the instability of a gas-liquid surface were performed by Taylor [2], who looked at the instabilities that can develop when an initial disturbed interface between two fluids is accelerated in a direction perpendicular to the interface. Lewis [3] designed an apparatus to accelerate various fluids at rates on the order of 50 times the acceleration of gravity and discovered that as the interface disturbance progresses, it begins to take the form of large round-ended columns of penetrating fluid.

Saffman and Taylor [4] made use of the Hele-Shaw analog developed in 1898. This analog states that the penetration of a fluid into a porous media is mathematically equivalent to the motion of a viscous fluid between two parallel plates separated by a very small gap, which corresponds to the experimental setup

in this study. Experimental studies led to the discovery of the dependence of finger shape and fractional coverage of finger on the capillary number Ca, which represents the ratio of viscous to surface tension forces in the flow. For Newtonian fluids, the finger width fraction as a function of capillary number resulted in a single master curve. Pitts [5] offered a theoretical account of the previous work and developed a theory to improve the agreement between the experimental results and theory presented by Saffman and Taylor. McLean and Saffman [6], in a similar work, attempted to resolve the indeterminacy of the growth of the Saffman-Taylor finger by introducing surface tension effects into the boundary conditions of the two-phase interface.

Park and Homsy [7] performed experiments on a single finger to investigate this proposed capillary number scaling, which was termed Ca', the modified capillary number. The researchers performed their own experiments as well as replotting the original work of Saffman and Taylor [4] based on the modified capillary number. The data from both research groups collapsed onto a single curve, which became the basis for concluding that the proposed scaling of McLean and Saffman was indeed correct. In addition, Park and Homsy [7] discovered that when the modified capillary numbers exceed 100 for a Newtonian fluid, the predominant finger undergoes a periodic tip splitting phenomena. The tip splitting pattern becomes more complex and loses its periodicity as the modified capillary number increases. Some more detailed theoretical and experimental studies of this hydrodynamic finger instability included works done by Saffman and Taylor

[8], Park et. al. [9], Saffman [10], and Park and Homsy [11].

Double asymptotic expansion was a technique employed in the theoretical study by Park and Homsy [11]. These results were compared to those experimentally obtained by taking pictures of the air bubble pushing its way through the displaced fluid in the experimental study by Park et. al. [9], the theory and experiments agreed well with each other within the measurement's accuracy. Spaid and Homsy [12-14] also studied rivulet instabilities in centrifugal spin coating of viscous Newtonian and non-Newtonian fluids. The spreading dynamics within this experiment involves interfaces between a solid, the air and a liquid.

Ackerman [15] built upon the work done by Park and Homsy as well as Saffman and Taylor to examine cell geometry and rheological effects on the gas bubble penetration in a Hele-Shaw cell. In the testing performed by Ackerman, a Newtonian, shear-thinning and Boger fluid were analyzed. It was found that the fluids exhibiting non-Newtonian properties reached an asymptotic width fraction less than that of the Newtonian case at high capillary numbers. Meanwhile, tip splitting characteristics of the shear thinning fluid were seen to be the least complex of the three fluids tested while the Boger fluid exhibited the most complexity.

The work done by Grimes et al. [16] examined Taylor and Bretherton laws regarding two-phase liquid flow in microchannels. In order to resolve discrepancies between the results collected for the two-phase liquid and data previously collected, a viscosity ratio of the core to shell fluid was incorporated

into the capillary number calculation in order to reach close agreement. Work has been done by Al-Housseiny et al. [17] in attempting to control the instabilities of both a gas-liquid and two immiscible liquid interface in a non-uniform Hele-Shaw cell by focusing on the critical capillary number where finger instabilities begin to form.

The goal of this work is to determine the effects of viscosity on a single finger of viscous fluid immiscibly penetrating a second viscous fluid in a Hele-Shaw cell. The viscosity of the penetrating bubble was adjusted to determine the effect on the bubble dynamics. The measured parameters were the width fraction of the bubble and the shape of the bubble formation as functions of modified capillary number and viscosity ratio.

Chapter 2: Materials and Methodology

2.1 Experimental Apparatus and Technique

Figure 1 is a cross-sectional view of the Hele-Shaw cell used during experimentation.

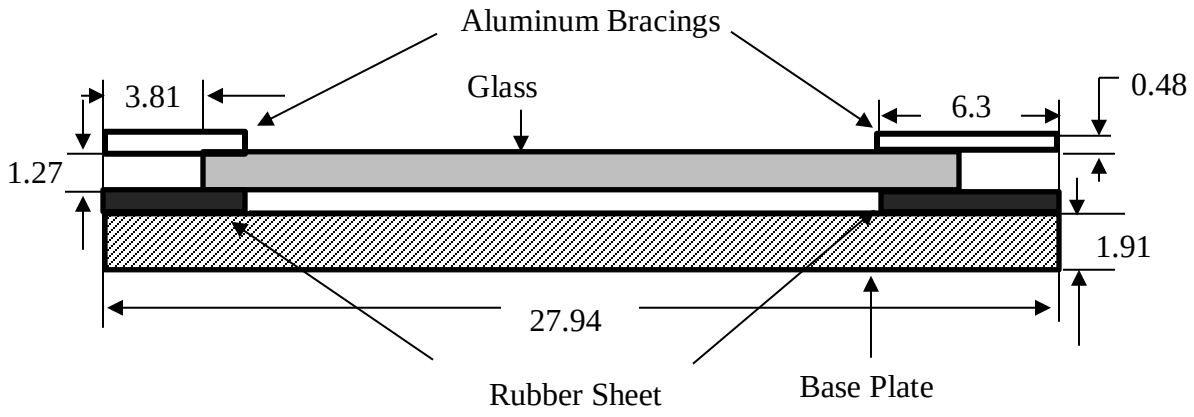

Figure 1: Cross section of assembled Hele-Shaw cell with relevant dimensions (cm)

The Hele-Shaw cell combines an aluminum base plate that is 27.94 x 109.22 x 1.905 cm with a glass plate that is 20.32 x 101.6 x 1.27 cm. The two plates are bolted together with aluminum bars at 12.7 cm intervals. Sandwiched between the two plates

lies a rubber sheet with a thickness of either 0.08 or 0.16 cm. A rectangle of 15.24 x 96.52 cm was cut out of the middle of the rubber sheet to create the space to allow the passage of fluid in the cell. An inlet tube with a 1 cm diameter was placed at one end of the plate and led to a channel with a width of 15.24 cm and a depth of 1.27 cm that was machined into the top surface of the base plate. Figure 2 shows the cross section of the two Hele-Shaw flow cells used in this study.

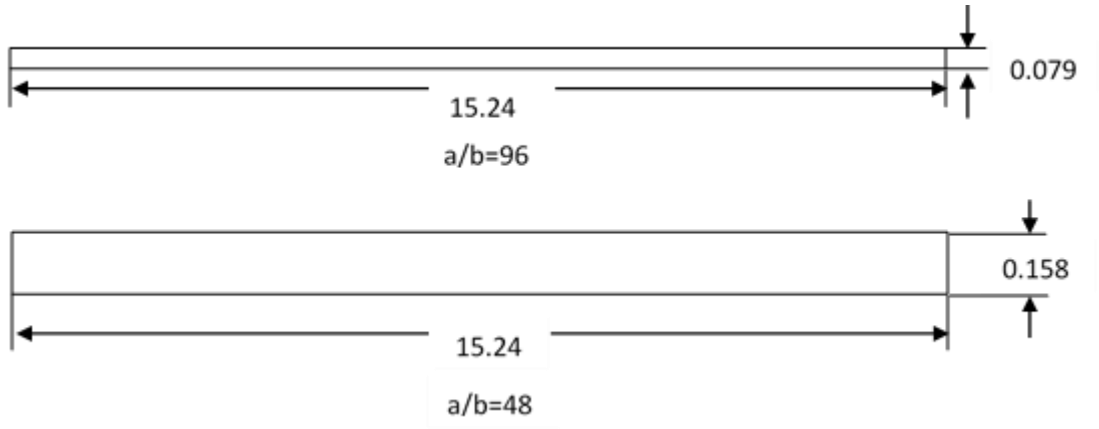

Figure 2: Cross sectional view of the two experimental Hele-Shaw cell setups

A Harvard apparatus syringe pump (model 919) was connected to the Hele-Shaw cell via stainless steel tubing. The syringe pump was used to fill the cell with the shell fluid prior to an experimental trial. Care was taken to remove any trapped air bubbles that remained after filling to prevent the bubbles affecting the flow development of the penetrating fluid.

After filling the cell with the shell fluid, a second syringe filled with the second fluid was attached for the secondary injection of the penetrating core fluid. The core fluid was injected at a specific volumetric flow rate that ranged between 1.2 and 120 cm^3/min. Displaced shell fluid would be driven out of the cell through a machined hole in the base plate at the far end of the cell.

To analyze the results, bubble progression was video recorded on a Google Pixel cell phone. The cell phone was mounted above the apparatus and the resulting video was used to calculate the velocity of the bubble as it travelled through the cell. A photograph would be taken at the end of each trial to calculate the stable width of the bubble. From the value of the width of the bubble, the thickness of the penetrating bubble would be calculated from the volumetric flow rate and duration of the trial as well as the length and width of the final bubble.

2.2 Fluid Characterization

For this experiment, the Newtonian case was the focus when performing trials. By studying the Newtonian case, the basis for future comparisons can be made when non-Newtonian fluids are incorporated. During testing the two immiscible liquid phases consisted of a mineral oil phase that was used as the displaced shell fluid and a water phase that would act as the penetrating fluid. Food coloring was used to dye the water phase to better define the boundary between the two phases. The surface tension between the two phases was obtained through literature to be 4.9 Pa*cm.

Two grades of mineral oil were used to run trials. The two grades used were CVS Health baby oil and Fisher Science Education light mineral oil. The viscosity of the water phase was adjusted by the addition of glycerol or Karo light corn syrup to meet the desired viscosity ratio between the two test phases. The dynamic viscosity of all fluids was tested through an Ostwald hydrostatic head viscometer and an MCR 500 rheometer using a couette geometry. These results are displayed in Table 1.

Table 1: Test fluid viscosities

Name	Viscosity (cP)
Oil Phase	
CVS Health Baby Oil	20
Fisher Education Light Mineral Oil	25
Water Phase	
Water	1
Water-Glycerol solution	5
Water-Corn Syrup solution	20

2.3 Width Fraction Experiments

The goal of these experiments was to determine the effects of Newtonian behavior on the bubble progression of the penetrating fluid. Figure 3 shows a schematic of a typical experiment highlighting the relevant variables needed in the analysis of the results.

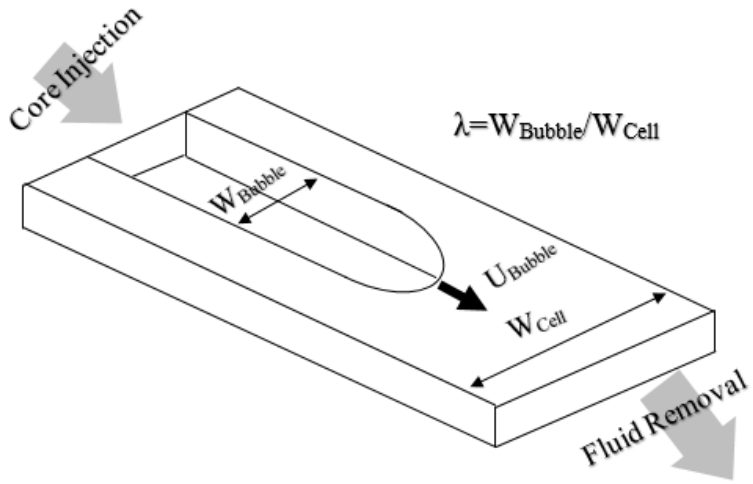

Figure 3: Representation of typical Hele-Shaw experiment with relevant variables

The measured parameter in these experiments was the bubble width fraction, λ, which is defined as:

$$\lambda = \frac{W_{BUBBLE}}{W_{CELL}} \tag{1}$$

where λ is the fraction of the cell width occupied by the penetrating bubble, W_{BUBBLE} is the width of the penetrating bubble and W_{CELL} is the width of the Hele-Shaw cell. The bubble width was measured as a function of the capillary number Ca, which represents the ratio of viscous forces to surface tension forces in the flow field:

$$Ca = \frac{U_B \eta_s}{\sigma} \tag{2}$$

where U_B is the penetrating bubble velocity, η_s is the dynamic viscosity of the Newtonian shell fluid and σ is the interfacial surface tension. For analyzing results from a Hele-Shaw setup and for this study, the modified capillary number, Ca', is used to to collapse the results on one single curve by multiplying the capillary number by a cell geometry factor such that:

$$Ca' = \frac{U_B \eta_s}{\sigma}\left(\frac{a}{b}\right)^2 \tag{3}$$

where $a=W_{CELL}/2$ and b is the thickness of the Hele-Shaw cell [7]. Figure 2 shows the cell geometries and corresponding a/b values used in this study. Since the geometry factor, dynamic viscosity and interfacial surface tension are known constants, the width

fraction, λ, and the penetrating bubble velocity, U_B were the only variables measured for each trial during experimentation.

Width fraction experimentation was broken down into two stages: experiments done with large differences in viscosities between the penetrating and shell fluids and experiments done with small differences in viscosities between the penetrating and shell fluids. When examining large viscosity differences between the penetrating and shell fluid and its effect on the developing bubble, the most extreme case would be the well-defined scenario where the penetrating bubble is an inviscid gas. Under this setup, the shell fluid is infinitely more viscous than its penetrating counterpart. To adjust this scenario for trials where both fluids are viscous, mineral oil (25 cP) was used as the shell fluid with water acting as the penetrating core fluid for a 1:25 viscosity ratio between core and shell. Results from these experiments were then compared with those done previously under the inviscid scenario. Trials performed at small viscosity differences between the penetrating and shell involved pairing the baby oil with the water-glycerol and water-corn syrup solutions for a 1:4 and a 1:1 respective ratio between core and shell viscosities.

Chapter 3: Experimental Results and Discussion

3.1 Width Fraction Results

3.1.1 Large Viscosity Differences between Penetrating and Shell Fluids

Figure 4 compares the results of a 1:25 viscosity ratio with those seen previously when studying the inviscid case.

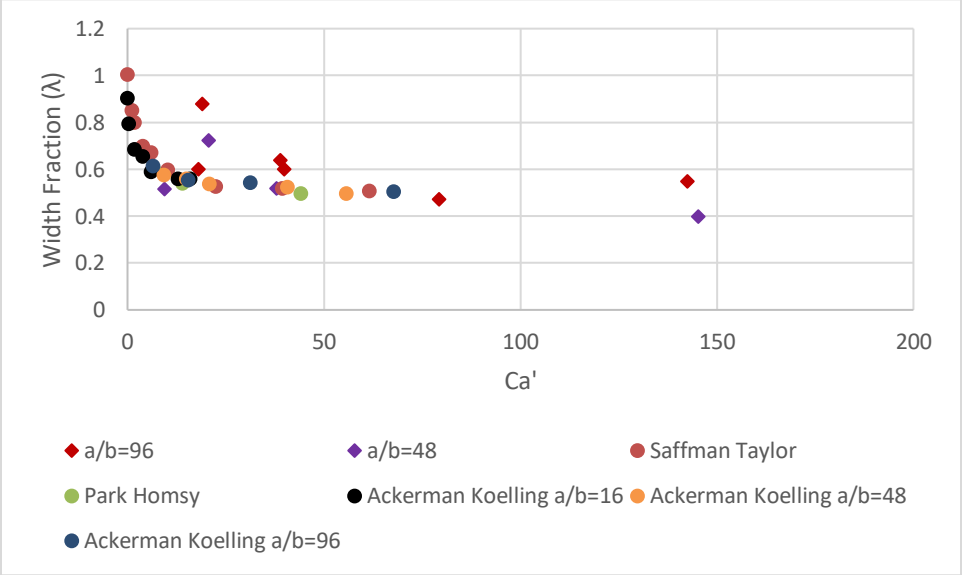

Figure 4: Comparison of λ vs. Ca' for inviscid case (circles) and a 1:25 viscosity ratio (diamonds)

Inviscid data was obtained from Saffman and Taylor [4], Park and Homsy [7], and Ackerman [15] as a reference when comparing the trends seen for large viscosity differences. A distinct separation is seen between the curves describing the inviscid case and the data collected in this study. This separation namely due to the scaling of the x-axis as the Ca' values are substantially larger due to the decrease in surface tension of a liquid-liquid interface rather than a liquid-air interface. To rescale the data collected, a second modified capillary number, Ca", is used by multiplying Ca' by the viscosity ratio of the core to shell fluids as done previously Grimes et al. [16]. Thus, Ca" becomes:

$$Ca" = \frac{U_B \eta_c}{\sigma} \left(\frac{a}{b}\right)^2 \tag{4}$$

with η_c representing the dynamic viscosity of the core fluid. Figure 5 reexamines the results of a 1:25 viscosity ratio as a function of Ca" with those seen previously when studying the inviscid case.

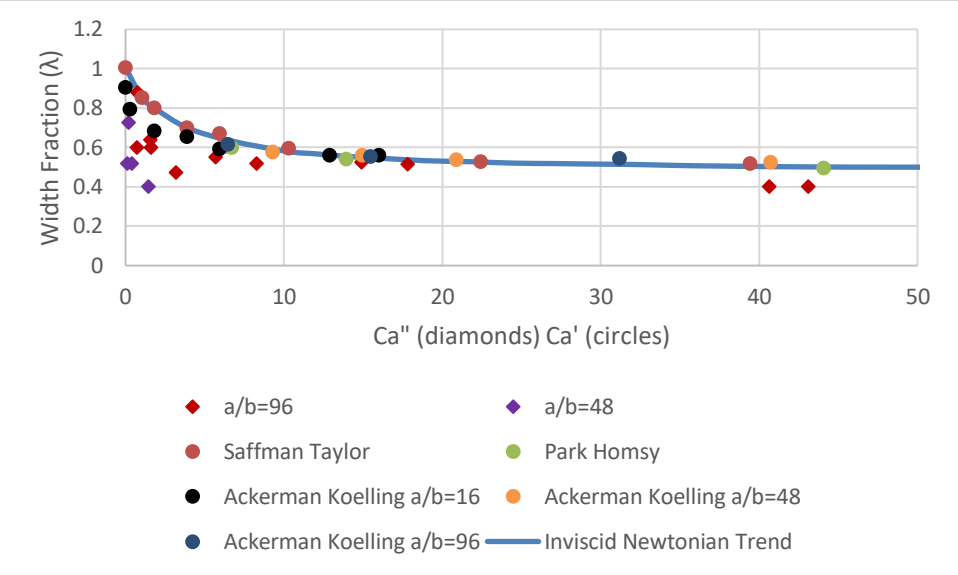

Figure 5: Comparison of λ vs. Ca' for inviscid case (circles) and λ vs. Ca" for a 1:25 viscosity ratio (diamonds)

When width fraction, λ, is plotted as a function of the modified capillary number, Ca', trials performed with the mineral oil-water interaction display similar trends to that of the inviscid data. Both setups show λ approach one as Ca' approaches zero and that λ will rapidly decrease before reaching an asymptotic value as Ca' increases. For large values of Ca' this asymptotic value is λ=0.5 based on previous studies. Meanwhile, an asymptotic value of λ=0.4 was observed for the mineral oil-water combination. Additionally, the data for the mineral-oil water interaction does not collapse onto a single curve when dealing with the geometric factor in Ca" as the results for a/b=48 reach the asymptotic value of 0.4 at a Ca" value much lower than that obtained by a/b=96.

3.1.2 Small Viscosity Differences between Penetrating and Shell Fluids

Figure 6 compares the results of a 1:4 and 1:1 viscosity ratio with those seen previously when studying the inviscid case.

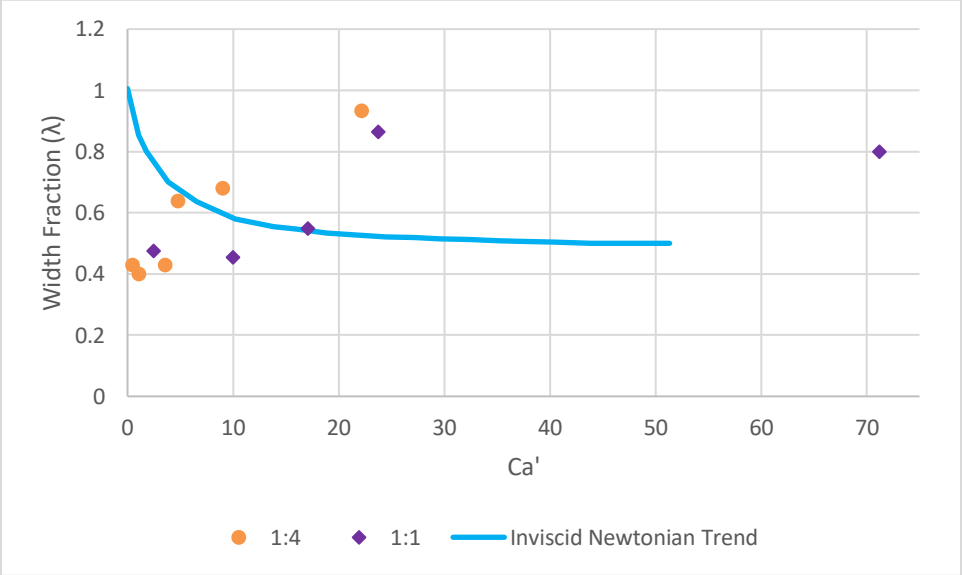

Figure 6: Comparison of λ vs. Ca' for inviscid case, 1:4 and 1:1 viscosity ratios

Both trials were conducted in the geometry a/b=48. The plot of λ as a function of Ca' no longer shows any resemblance to that of the inviscid trend as the viscosity of the penetrating water phase approaches the viscosity of the oil phase. Rather than λ approaching one as Ca' approaches zero, the starting value of λ=0.4 is the same as that of the asymptotic value seen in the results of a large viscosity difference. The value for λ then increases as Ca' increases. Based on the data obtained, the value of λ should reach

an asymptotic value close to its maximum of $\lambda=1$ at large values of Ca'. Future studies at high Ca' values are needed in order to better investigate this trend.

3.2 Bubble Progression Characteristics

3.2.1 Instabilities and Tip Splitting

The progression of bubble penetration in a Hele-Shaw cell is marked by three distinct regimes based on the shape of the penetrating bubble: stable, unstable, and tip splitting. In the experiments performed by Ackerman, it was determined that for the inviscid case the stable regime exists at Ca' values less than 100 while splitting occurs at Ca' values greater than 300 [15]. Figure 7 contains images from that study of the bubble progression with increasing capillary number.

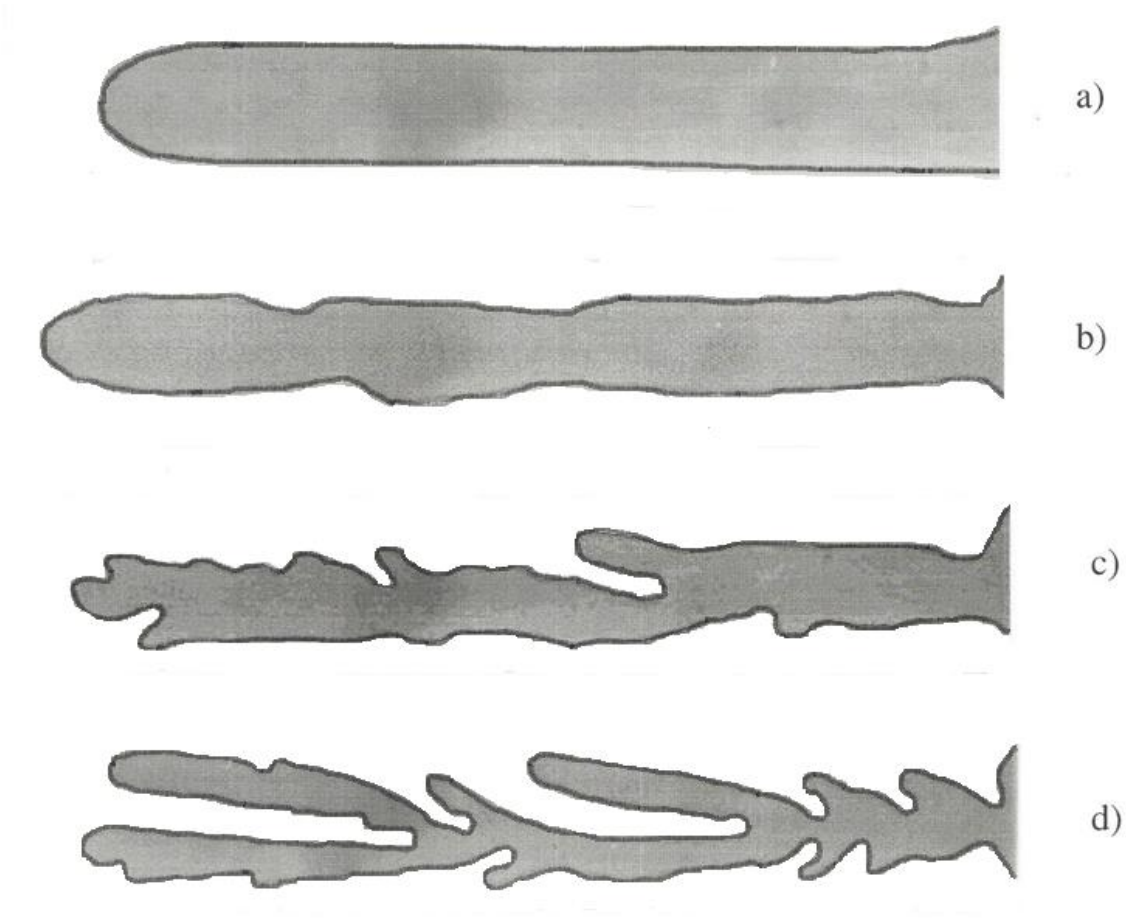

Figure 7: Air bubble penetration through Newtonian fluid at modified capillary numbers (Ca') of 10 (a, stable), 100 (b, unstable), 300 (c, tip splitting), 700 (d, tip splitting)

Comparatively, instabilities began to appear in the liquid-liquid system at a Ca" value above 0.2 and reached tip splitting starting at a Ca" value of 40.

Figure 8 shows a comparison of the bubble formation in each regime for a 1:25 viscosity ratio between core and shell fluid.

Figure 8: Bubble penetration of water through mineral oil at modified capillary numbers (Ca") of 0.2 (a, stable), 0.4 (b, unstable), 40 (c, tip splitting) 1:25 viscosity ratio

Both the instability and tip splitting regions begin at lower Ca" values compared to the critical Ca' for the inviscid system as well as appearing independent of the viscosity ratio

between the two fluids in the liquid-liquid system. It is worth noting that the image of a stable water bubble is the only one seen in this study and further investigation needs to occur to properly explore this regime.

Additionally, a couple preliminary trials examined what the bubble progression would look like if the penetrating core fluid was more viscous than the displaced shell fluid. Figure 9 shows the typical result from these investigative trials with 20 cP mineral oil being injected moving left to right with water (dyed with food coloring) as the displaced fluid.

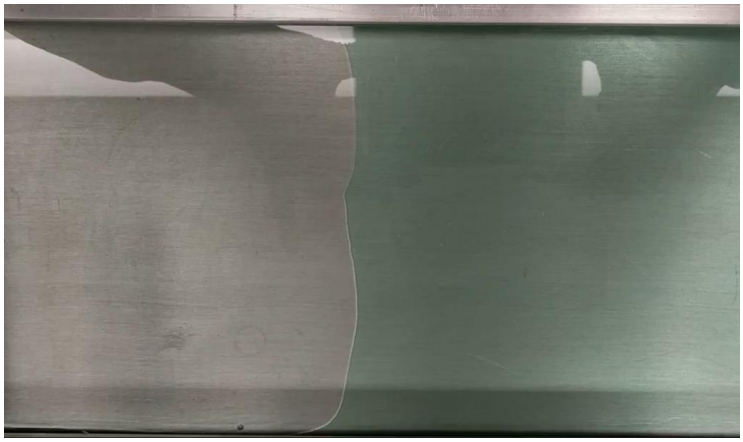

Figure 9: Bubble penetration of mineral oil through water (20:1 viscosity ratio)

In this scenario the core fluid has a width fraction of one and appears as a moving wall of fluid with only minor instability.

3.2.2 Development of Secondary Front in Fluid Flow

During the trials with a viscosity ratio of 1:1, it was observed that trailing the penetration of the initial bubble, a secondary front would form filling up the width of the cell and forming a wall behind the leading bubble. This phenomenon was initially seen at a Ca" value of 10 and continued for the remainder of the trials increasing in Ca" value. Figures 10-13 show the results of the secondary fronts for each trial observed.

Figure 10: Secondary front at Ca"=10

Figure 11: Secondary front at Ca”=17

Figure 12: Secondary front at Ca”=24

Figure 13: Secondary front at Ca”=71

As Ca” increases, the distance between bubble tip and the secondary front decreases. The presence of the secondary front also appears to decrease the instabilities seen in the developing bubble until the tip splitting regime is reached. For the purpose of calculating width fractions for these trials, the width of the leading bubble was used rather than the value for the secondary front.

Chapter 4: Conclusions

Through investigating the interaction between two immiscible liquid phases in a Hele-Shaw cell, several distinct differences were observed in comparison to studies performed under inviscid conditions. Plotting width fraction as a function of modified capillary number resulted in the formation of different curves in comparison to data obtained from inviscid experiments. In order to rescale the data to match the inviscid trends, a second modified capillary number was used by incorporating the viscosity ratio between the core and shell fluids in accordance to Grimes et al. [16]. Upon rescaling, data obtained with large viscosity differences between the two fluids was found to be in close agreement with the inviscid case with the exception being a lower asymptotic value of 0.4 compared to 0.5. Meanwhile, data obtained with smaller viscosity differences between core and shell fluids was shown to increase with an increase in capillary number such that the width fraction approached 0.4 as Ca" approached zero and reached an asymptotic value close to its maximum of one as Ca" increased.

The visual regimes in bubble progression seen under inviscid conditions remained when operating with a liquid bubble. In maintaining Ca" as a liquid-liquid equivalent to compare against Ca' under inviscid conditions, the separation between stable, unstable and tip splitting regimes was observed to occur at lower Ca" values compared to its Ca' counterpart with a gas bubble. Lastly, a new regime was observed when conducting trials

with equivalent viscosities between the core and shell fluids. Under this regime a secondary flow front developed behind the leading, penetrating bubble resulting in a wall occupying the width of the cell.

Chapter 5: Future Work

In order to achieve the overall goal of accurately representing industrial processes through the 2-D analog of a Hele-Shaw cell, this study should be expanded upon in the following ways: inclusion of more viscosity ratios, testing performed at a more extensive range of capillary numbers, and investigation into the non-Newtonian regime. Due to the distinct discrepancy in the relationship of λ as a function of Ca" when comparing large and small differences in the viscosities of the two fluids further evaluation needs to occur to determine the critical viscosity ratio that separates these two trends as well as observing what occurs as the difference in viscosities approaches this ratio. Comprehensive testing throughout a wider range of capillary numbers will serve to better examine tip splitting formations as well as providing an accurate determination of the critical Ca" values that separate the three regimes in bubble penetration. Finally, the addition of the complexities associated with the incorporation of non-Newtonian under this experimental setup will provide the most accurate representation of industrial processes to maximize the impact and utility of this study.

References

[1] Boger, D.V., The Influence 0f Rheological Properties on Mobility Control in Polymer Augmented Waterflooding. (1988). 63rd ANTEC of Society of Petroleum Engineers, Houston TX 449-456.

[2] Taylor, G., Instability of Liquid Surfaces when Accelerated in a Direction Perpendicular to Their Planes. (1950). Proc Roy Soc. A, 201, 192-196.

[3] Lewis, D.J., The Instability of Liquid Surfaces when Accelerated in a Direction Perpendicular to Their Planes. Parts I&II. (1950), Proc. Roy. Soc. A, 202, 81-96.

[4] Saffman, P. G. and Taylor, G, The Penetration of a Fluid into a Porous Medium or Hele-Shaw Cell Containing a more Viscous Liquid. (1958), Proc. Roy. Soc. A, 245, 312-329.

[5] Pitts, E., Penetration of Fluid into a Hele-Shaw Cell: the Saffman-Taylor Experiment. (1980), J Fluid Mech., 97, 53-64.

[6] McLean, J.W. and Saffman, P.G., The Effect of Surface Tension on the Shape of Fingers in a Hele-Shaw Cell. (1981) J. Fluid Mech., 102, 455-469.

[7] Park, C.W., and Homsy, G.M., The Instability of Long Fingers in Hele-Shaw Flows. June (1985), Phys. Fluids 28 (6), 1583-1585.

[8] Taylor, G. and Saffman, P.G., A Note on the Motion of Bubbles in a Hele-Shaw Cell and Porous Media. (1959), Quart. Journ. Mech. And Applied Math, 12, 265-279.

[9] Park, C.W., Gorell, S., and Homsy, G.M., Two -phase Displacement in Hele-Shaw Cells: Experiments in Viscously Driven Instabilities. (1984), J. Fluid Mech., 141, 257- 287.

[10] Saffman, P.G., Viscous Fingering in Hele-Shaw Cells. (1986), J. Fluid Mech., 173, 73- 94.

[11] Park, C. W., and Homsy, G. M., Two-Phase displacement in Hele-Shaw cells: theory. J.Fluid Mech.(1984), vol. 139. pp.291-308.

[12] Spaid, M. A., Homsy, G. M., Viscoelastic free surface flows: spin coating and dynamic contact lines. J.Non-Newtonian Fluid Mech. (1994), 55(3), 249-81. CODEN: JNFMDI; ISSN: 0377-0257. CAN 122:109787 250

[13] Spaid, M.A., Homsy, G.M., Stability of Newtonian and viscoelastic dynamic contact lines. Phys. Fluids (1996), 8(2), 460-78. CODEN: PHFLE6; ISSN: 1070-6631. CAN 124:98358

[14] Spaid, M.A.; Homsy, G.M., Stability of viscoelastic dynamic contact lines: an experimental study. Phys.Fluids (1997), 9(4), 823-832. CODEN: PHFLE6; ISSN: 1070-6631. Can 127: 23918

[15] Ackerman, J.D., "Fluid rheology and mold geometry influence on fingering in gas-assisted injection molding", The Ohio State University: M.S. Thesis, 1996

[16] Grimes, R., King, C., and Walsh, E., 2007, "Film Thickness for Two Phase Flow in a Microchannel, Advances and Applications in Fluid Mechanics", 2 (1), pp. 59-70.

[17] Al-Housseiny, T., Tsai, P., and Stone, H., 2012, "Control of interfacial instabilities using flow geometry", Nat Phys 8:747–750

[18] Wang, Y., "The Effect of Non-Newtonian Rheology on Gas-Assisted Injection Molding Process", The Ohio State University: PhD Thesis, 2003

Appendix A: Images of Bubble Progression

Testing at a 1:1 viscosity ratio:

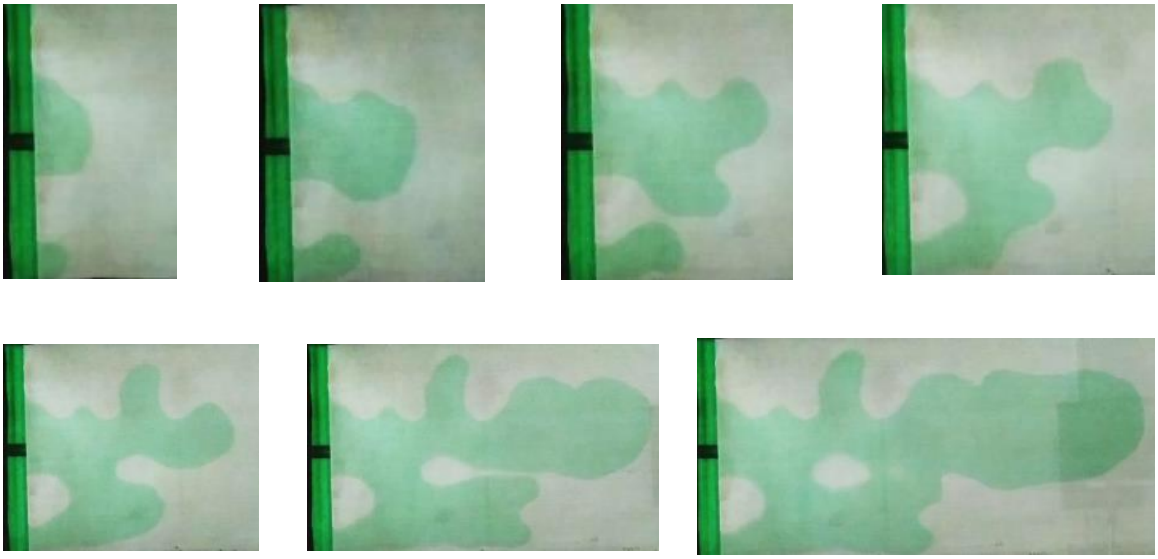

Entrance flow to steady bubble (Ca”=2.5)

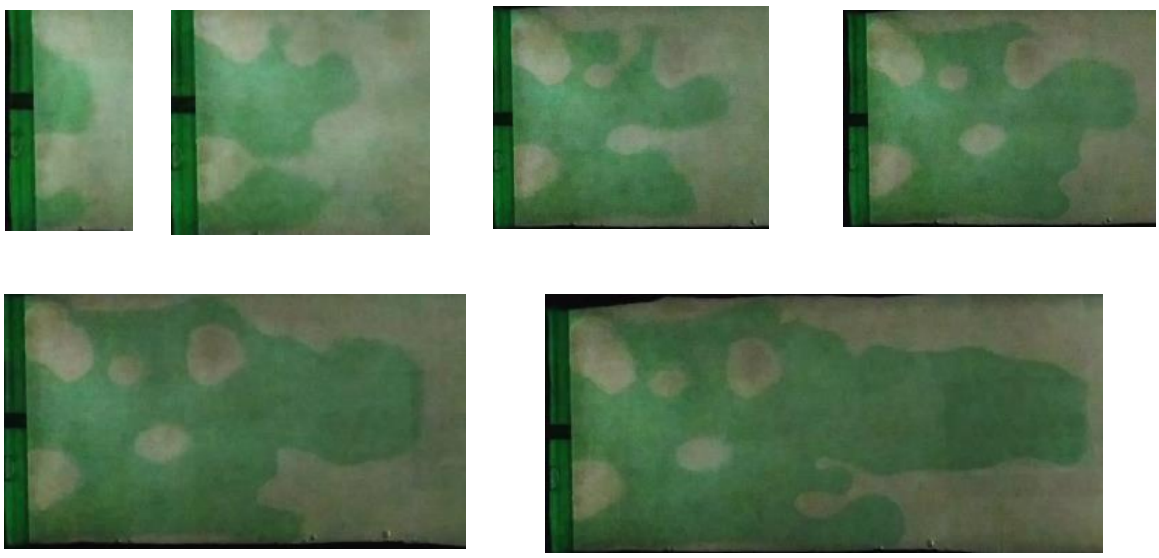

Entrance flow to steady bubble (Ca”=10)

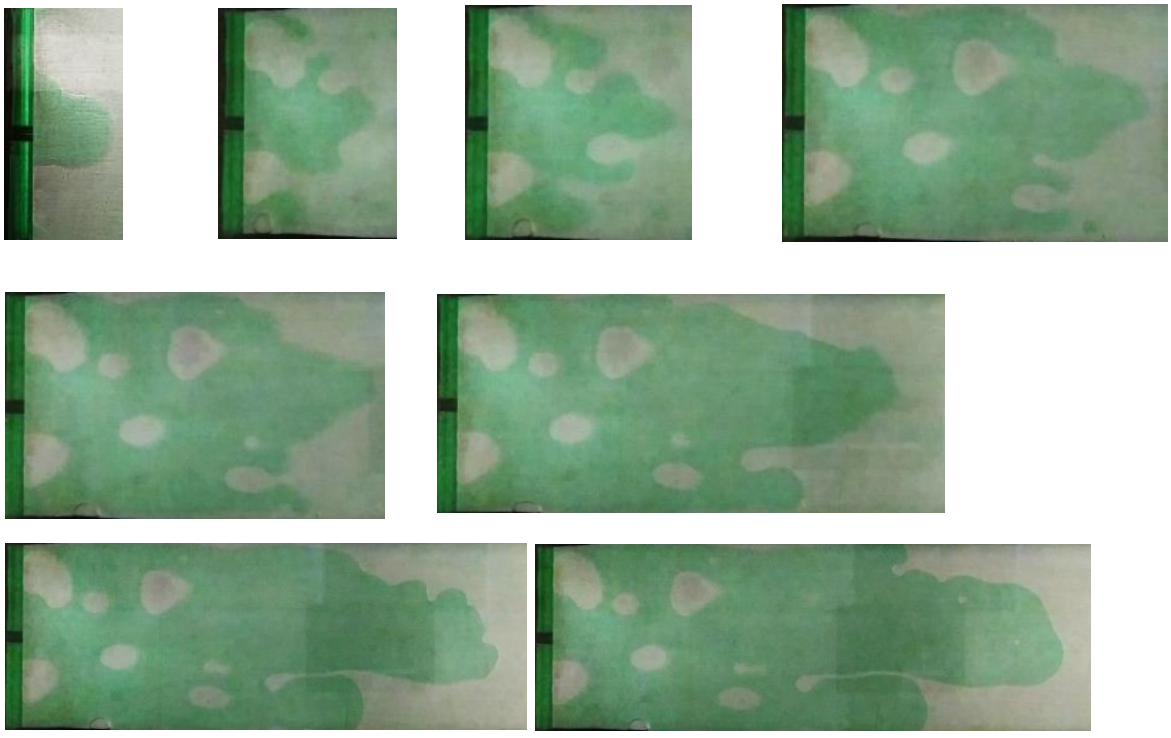

Entrance flow to steady bubble (Ca”=17)

Testing at a 1:4 viscosity ratio:

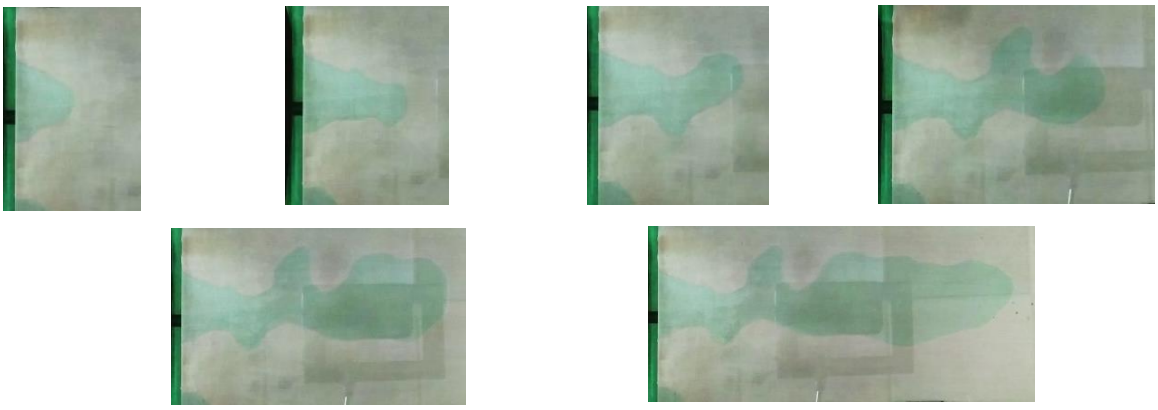

Entrance flow to steady bubble (Ca”=0.5)

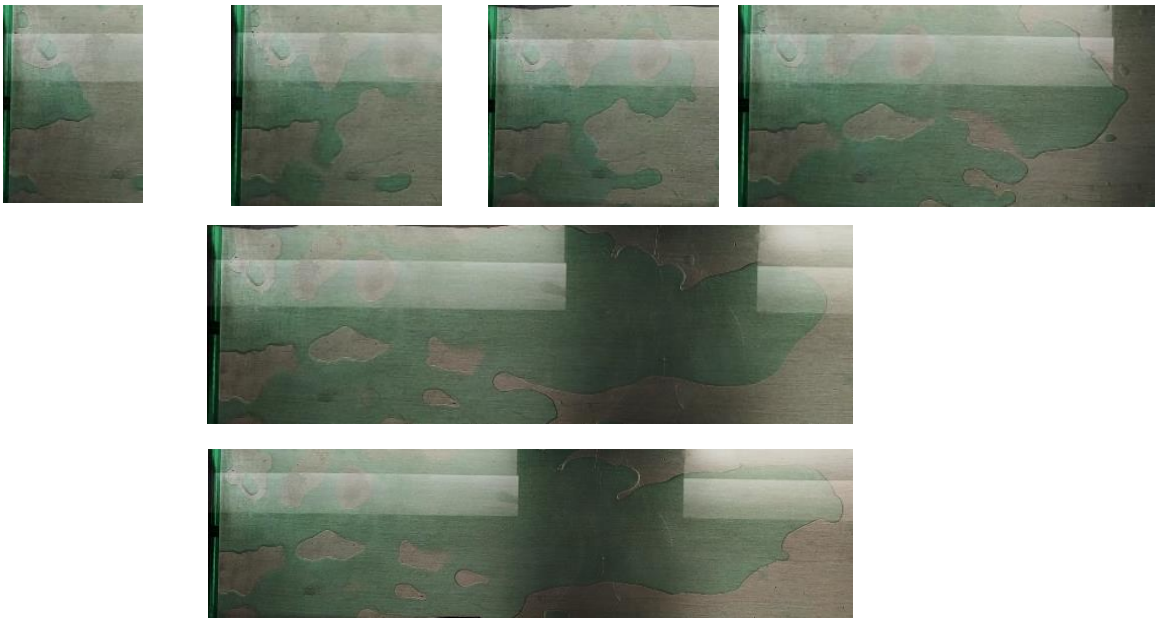

Entrance flow to steady bubble (Ca”=9)

Testing at a 1:25 ratio:

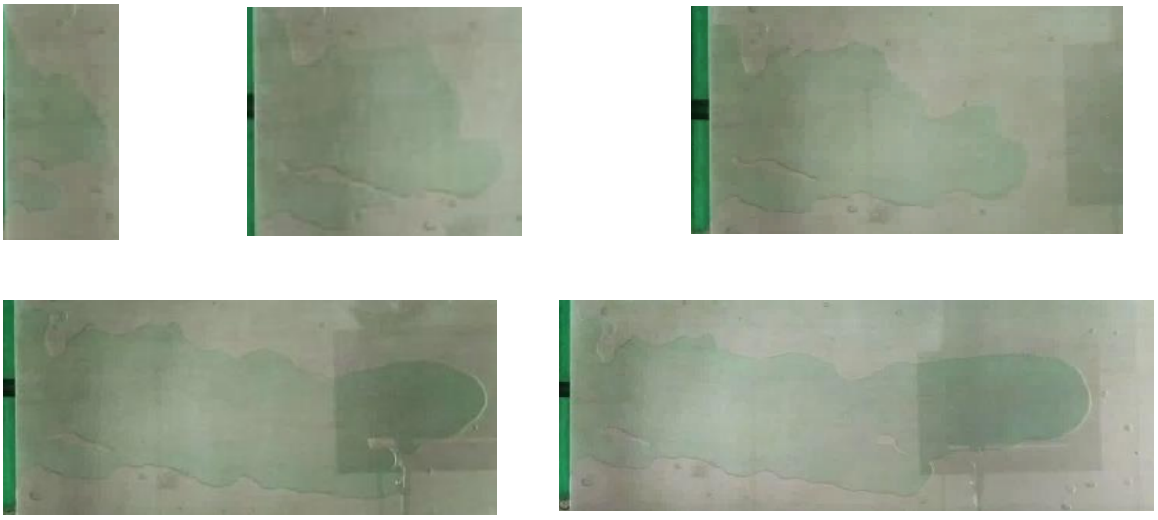

Entrance flow to steady bubble (Ca”=8.25)

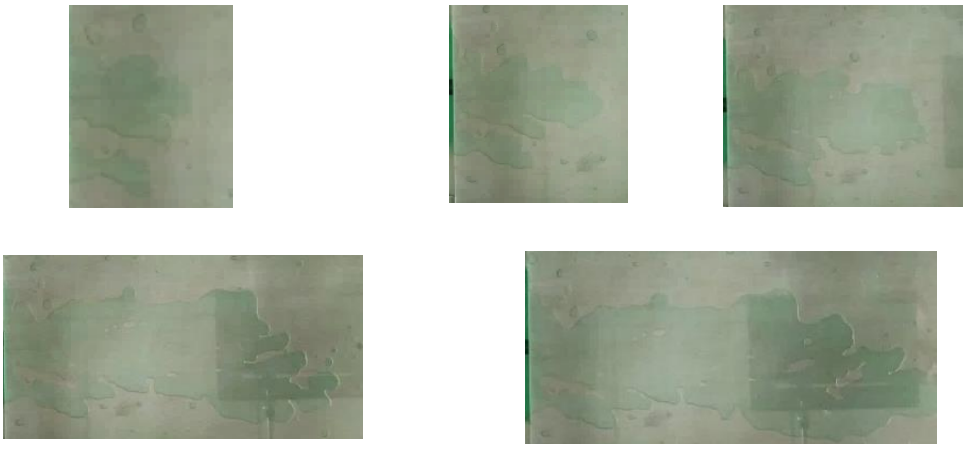

Entrance flow to steady bubble (Ca”=17.8)